Influence of Nd and Ce doping on the structural, optical and electrical properties of V_2O_5 thin films

I. K. Jassim[1], Jamal M. Rzaij[2], Iftikhar M. Ali[3], Isam M. Ibrahim[3]

[1]Department of Physics, College of Education, Tikrit University

[2]Department of Physics, College of Science, Al Anbar University

[3]Department of Physics, College of Science, Baghdad University

E-mail: ismail_khalil1956@yahoo.com

Abstract

Nano-structural of vanadium pentoxide (V_2O_5) thin films were deposited by chemical spray pyrolysis technique (CSPT). Nd and Ce doped vanadium oxide films were prepared, adding Neodymium chloride ($NdCl_3$) and ceric sulfate ($Ce(SO_4)_2$) of 3% in separate solution. These precursor solutions were used to deposit un-doped V_2O_5 and doped with Nd and Ce films on the p-type Si (111) and glass substrate at 250°C. The structural, optical and electrical properties were investigated. The X-ray diffraction study revealed a polycrystalline nature of the orthorhombic structure with the preferred orientation of (010) with nano-grains. Atomic force microscopy (AFM) was used to characterize the morphology of the films. Un-doped V_2O_5 and doped with 3% concentration of Nd and Ce films have direct allowed transition band gap. The mechanisms of dc-conductivity of un-doped V_2O_5 and doped with Nd and Ce films at the range 303 K to 473 K have been discussed.

Key words

Vanadium oxide, thin films, structural properties, electrical properties.

Article info.

Received: Jan. 2016
Accepted: Mar. 2016
Published: Sep. 2016

تأثير التطعيم بالنديميوم والسيريوم على الخصائص التركيبية والبصرية والكهربائية لأغشية اوكسيد الفناديوم

اسماعيل خليل جاسم[1]، جمال مال الله رزيج[2]، افتخار محمود علي[3]، عصام محمد ابراهيم[3]

[1]قسم الفيزياء، كلية التربية، جامعة تكريت

[2]قسم الفيزياء، كلية العلوم، جامعة الانبار

[3]قسم الفيزياء، كلية العلوم، جامعة بغداد

الخلاصة

اغشية اوكسيد الفناديوم الرقيقة ذات التركيب النانوي قد تم ترسيبها بتقنية الرش الكيميائي، كما تم تطعيم اغشية اوكسيد الفناديوم بالنيديميوم Nd والسيريوم Ce بإضافة كلوريد النيديميوم وكبريتات السيريوم بنسبة 3% لكل من Nd و Ce في محلولين منفصلين. ورسبت الاغشية على ارضية من السليكون نوع N ذات التوجه بلوري (111) وارضيات من الزجاج وبدرجة حرارة اساس 250 °C. تم اجراء الفحوصات التركيبية والبصرية والكهربائية حيث اظهرت نتائج فحوصات الاشعة السينية ان العينات لها تركيب متعدد التبلور ومعيني قائم وبدورانية (010) وبحجم نانوي. كما تمت معرفة خواص السطح بإجراء فحوصات مجهر القوة الذرية. تمتلك اغشية V_2O_5 النقية والمطعمة بالنيديميوم Nd والسيريوم Ce فجوة طاقة مباشرة مسموحة كما نوقشت ميكانيكيه التوصيلية المباشرة للأغشية المحضرة.

Introduction

One goal of today's technology is the miniaturization of the electronic, actuating, sensing, and optical devices and their components; hence, nanotechnology is an advanced technology that has received a lot of attention from the worlds of the science and industry for its ability to make use of the unique properties of nanosized materials. Nanotechnology is capable of manipulating and controlling material structures at the nano level (a nanometer is equal to one millionth of a millimeter) and offering unprecedented functions and excellent material properties [1].

Vanadium oxide is of enormous research interest because of its multivalent nature. The vanadium oxides exist in the V^{2+}, V^{3+}, $V^{4+}$and V^{5+} oxidation states and form the VO, V_2O_3, VO_2 and V_2O_5 materials [2]. Among these, vanadium pentoxide (V_2O_5) has drawn significant interest over the past decades owing to its wide range of applications. Its multivalency, layered structure, wide optical band gap, good chemical and thermal stability, excellent thermoelectric property, etc., are the characteristics that make vanadium pentoxide (V_2O_5) a promising material for applications in microelectronics, and for electrochemical and optoelectronic devices. It can be used as a catalyst, gas sensors, a window for solar cell and electrochromic devices as well as electronic and optical switches [3]. V_2O_5 is the most stable oxide and show semiconductor property with an energy gap of ~2.2 eV at room temperature, and displays electrochromic properties with varying color from blue to green and yellow within two seconds upon charging/discharging [4].

Vanadium pentoxide films have been prepared using various physical and chemical techniques such as, spray pyrolysis [5-7], electron beam evaporation [8], thermal evaporation [9], pulsed laser deposition [10], and sol-gel [11] methods. Different literature reviews were added to study the structural, optical and electrical properties of Vanadium pentoxide thin films. Structure and semiconducting properties of amorphous vanadium pentoxide obtained by splat cooling[12]. Structural and optical studies for V_2O_5 thin films. The films gave two-step electrochromism, yellow to green and then green to blue [3]. Amorphous and crystalline of V_2O_5 thin films growled onto glass substrates with different concentrations from 0.1M to 0.5M Optical analyses showed the absorption coefficient shifts towards lower energies [13]. Developed a method of a facile synthesis for preparing nano-sized of V_2O_5 for high-rate lithium batteries using vanadyl oxalate in air [14]. In the present paper, un-doped vanadium pentoxide and doped with Nd and Ce thin films have been prepared by (CSPT) to produce large area and uniform coating [15].

Experimental procedure

Before starting the deposition, the solutions according to the films components was mixed then put it on the magnetic stirrer for about 15 minutes to be sure that the mixture solutions are mixed properly. Prior to deposition, Si substrates (for studying the structural properties) and glass substrates (for studying the optical and electrical properties) were cleaned and places on the flat plate heater surface, which it is an electrically controlled, and leaves them for about 10 minutes so as to allow their temperature to reach the set temperature at (250 ± 5)$^{\circ}$C. After that, can start the deposition process within deposition time of 5 sec, and then stop this process for 10 sec. In the spray system, compressed and purified air was used

as the carrier gas with a 3 kg/cm^2 pressure and the solution spray rate was maintained at 3 ml/min. The distance between the spray nozzle and the substrate was fixed at 30 cm. After the spray process is completed, then the hot plate will be shut down and the samples are left on the surface of the heater to reach the room temperatures, then the substrates can be raised.

The X-ray diffraction (XRD) spectra of the films were obtained to verify their crystal structure using a (Cu-Kα) radiation with λ = 0.154 nm. Optical transmission data were obtained using an UV-Vis double beam spectrometer at wavelengths ranging from 200 nm to 900 nm. Atomic force microscopy (AFM) was employed to observe the surface morphology of the films. The resistance of the films was measured with the two-point probe method using sensitive digital electrometer type Keithley (616) in the temperature range of 30 °C to 200 °C.

Results and discussion

Structural properties

X-ray diffraction pattern of the prepared V_2O_5 Un-doped and doped with 3% concentration of Nd and 3% of Ce compound on Si substrate at T_s=250°C, is shown in Fig.1, it is indicate to a high intensity and sharp peak at 2θ=28°, it is attributed to the crystalline Si substrate with crystalline plane (111).

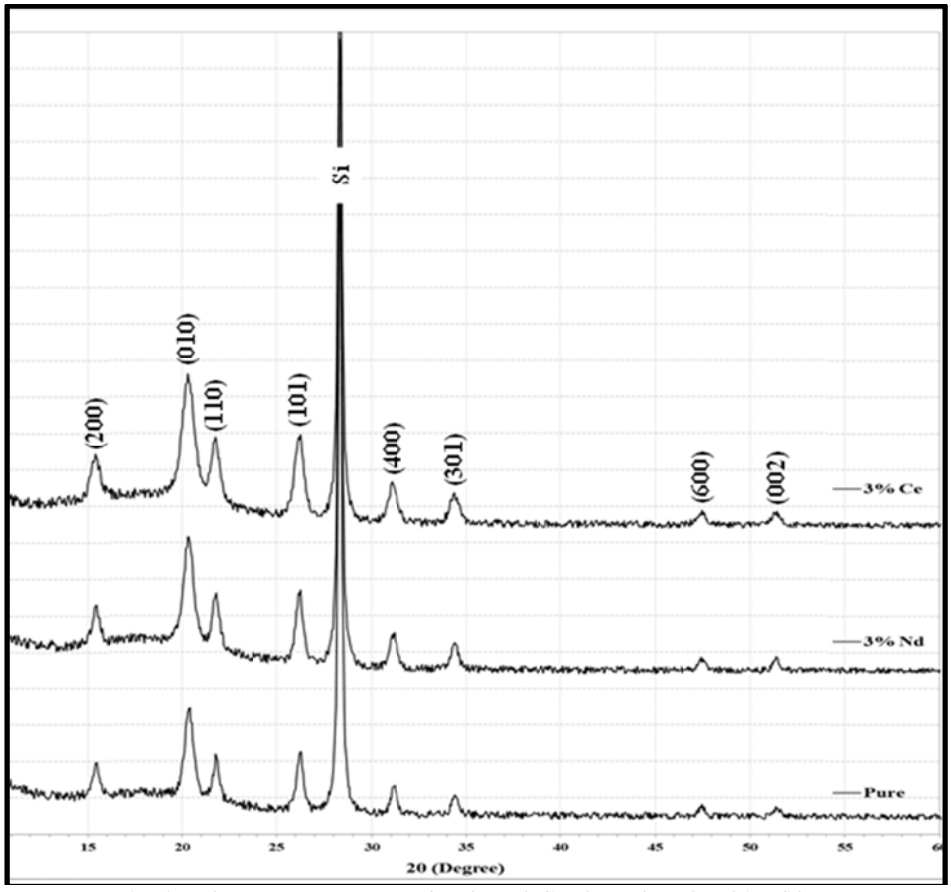

Fig.1: The XRD pattern of Nd and Ce doped V_2O_5 thin films.

The obtained XRD patterns possess polycrystalline vanadium pentoxide structure with planes (200), (010), (110), (101), (400), (301), (600) and (002) which in agreement with [13,16]. The films are crystallized in orthorhombic phase according to International Centre for Diffraction

(ICDPDF No.96-101-1226), which in agreement with [2,17,18,19]. The presents a preferential orientation of the film was along the plane (010) at diffraction angle of 2θ =20.36°, d =4.35 nm and lattice-parameter values of a=11.4734 Å, b=4.35809 Å and c=3.5533 Å. It is very close to the result obtained in [17,20]

The average crystallite size was equal to 26.29 nm. It was estimated with the Debye-Scherrer formula for the (010) reflection as follow:

$$D = \frac{0.94\lambda}{\beta \cos\theta} \qquad (1)$$

where λ is the wavelength of XRD photons which equal to 0.154 nm,β is the full-width at half maximum (FWHM) and θ is the Bragg diffraction angle in degrees.

There was increasing in the intensity of peaks diffraction with doping of both Nd and Ce. Not to appearance of new phases for a new compound which returns to the doping material in XRD diagram at these ratios. That may be due to the low proportion of neodymium and cerium that were doped, so it is difficult to be discovered in the examination of (XRD). The structure of prepared films are still as polycrystalline after doping with Nd and Ce, in addition to that increase in the (010) peak intensity may be attributed to the formation of new nucleating centers due to the dopant atoms resulting from the decrease of nucleation energy barrier.

We can observe from Fig.1, an increase in the FWHM and which consequently leads to a decrease in crystallite size with doping ratio for Nd and Ce, as a comparison of pure vanadium pentoxide films according to Eq. (1), where the relation between the crystallite size and FWHM is reverse. Decreasing in the crystallite size after doping is evidence on the improvement of the nano crystal, which indicates that the deposited atoms of these films going towards nanostructure. There was a decrease in the D value when V_2O_5 films doped with Nd and Ce dopant which indicate to nanoparticles formed which it was resulting from the doping process.

Three-dimensional AFM images and the chart of grain density distribution for V_2O_5:Nd and Ce are shown in Fig.2. AFM images were taken in order to further observe microstructure and confirm the XRD result. The average diameter, average roughness and root mean square roughness (r.m.s) are deduced from AFM images. The finer morphology and roughness of the films can be clearly seen. We can conclude that the grain size is uniform. The photography of AFM reveals a uniform growth of the film. The AFM images displayed all samples are granular structure.

Morphology parameters include average diameter, average roughness, average r.m.s roughness and peak – peak for samples are tabulated as shown in Table 1. AFM analysis for un-doped V_2O_5 film showed there is much bigger quasi bar-shape grains formed in the film, also it has a good uniformity revealing a uniform growth of the films.

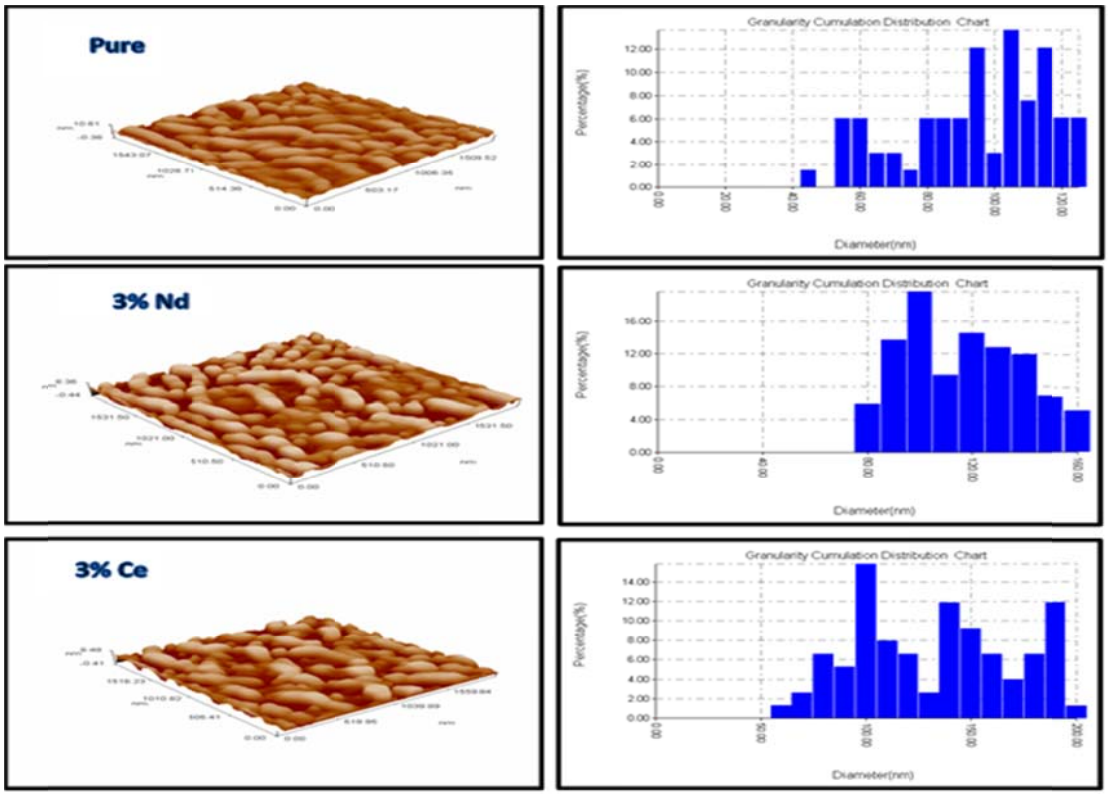

Fig.2: AFM images and Size distributions for V_2O_5 at 3% doping ratios of Nd and Ce.

Table 1: Morphology parameters for un-doped V_2O_5 and doped with 3% concentration of Nd and Ce.

Sample	Average diameter (nm)	Average roughness (nm)	r.m.s roughness (nm)	Peak –Peak (nm)
0%	127.91	1.5	1.98	19
3% Nd	122.1	2.43	2.82	13.1
3% Ce	111.38	1.57	1.8	7.56

The roughness of these films increases due to the existence of many hillocks, which are faceted and distributed randomly on the relatively smooth surface, so the increase of roughness can be explained by the grain growth and some structure densification of the deposition processes [21].

Optical properties

Optical energy gap (E_g)

The type of transition was directly allowed transition because the dependence of (α) on the photon energy (*hν*) was found to obey the following relationship:

$$\alpha h\nu = \beta\left(h\nu - E_g\right)^{\frac{1}{2}} \qquad (2)$$

where β is a constant and E_g is the optical band gap.

A plot of $(\alpha h\nu)^2$ versus *hν* shows the optical band gap of films with direct transition, as shown in Fig. 3. The optical energy gap for un-doped V_2O_5 films is about (2.2) eV. This result is reasonable and is very close to other (E_g) values found in literature [4,22,23].

It can be observed that (E_g) is increasing slightly and shifting towards the ultra-violate region as the doping with Nd and Ce.

This is because of the effect of impurity or disorder and any other defects in semiconductors leads to local electric fields that affect the band tails near the band edge [24]. Also the size effect for nanostructure makes this shift. The results of optical energy gap indicate that all the films have localized states which result from the density of defects at the grain boundaries and donor levels, so we can conclude that the optical energy gap can be controlled through the control of impurities ratios and the size of nanostructure.

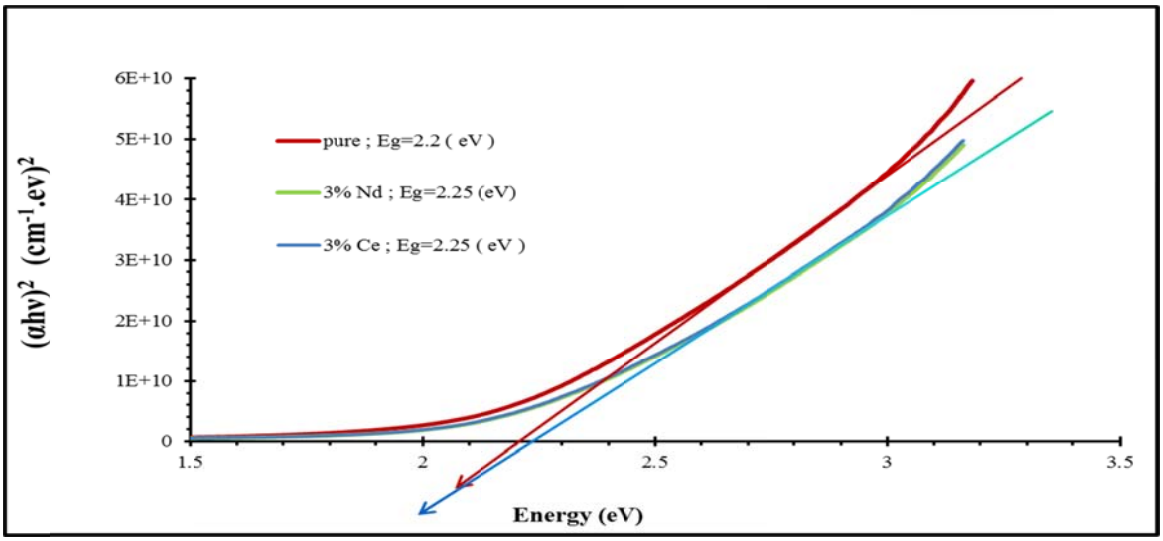

Fig. 3: Tauc plot for un-doped V_2O_5 and doped with Nd and Ce at 3% concentrations.

Electrical properties

Films were tested to confirm their semiconducting behavior. The film is placed on the heater and their resistances are measured in the range from 30 °C up to 200 °C, with step of 10 °C, in the dry air atmosphere. Fig. 4 shows the variation of resistance with temperature for un-doped and doped V_2O_5 films with 3% of Nd and 3% of Ce as a ratio of dopant. The films display high resistance at lower measuring temperature, and the resistance of the films decreased as the measuring temperature increasing which is a semiconductor behavior. The temperature in the range 30 °C to 90°C for un-doped V_2O_5 and doped films shows a typical negative temperature coefficient of resistance due to thermal excitation of the charge carriers in the semiconductor [25,26].

The variation of activation energy for V_2O_5:Nd and Ce with the ratio of 3% films is summarized in Table 2. The plot of ln(σ) versus 10^3/T in the range of (303-473) K and temperature deposited at 250 °C on a glass substrate is shown in Fig. 5.

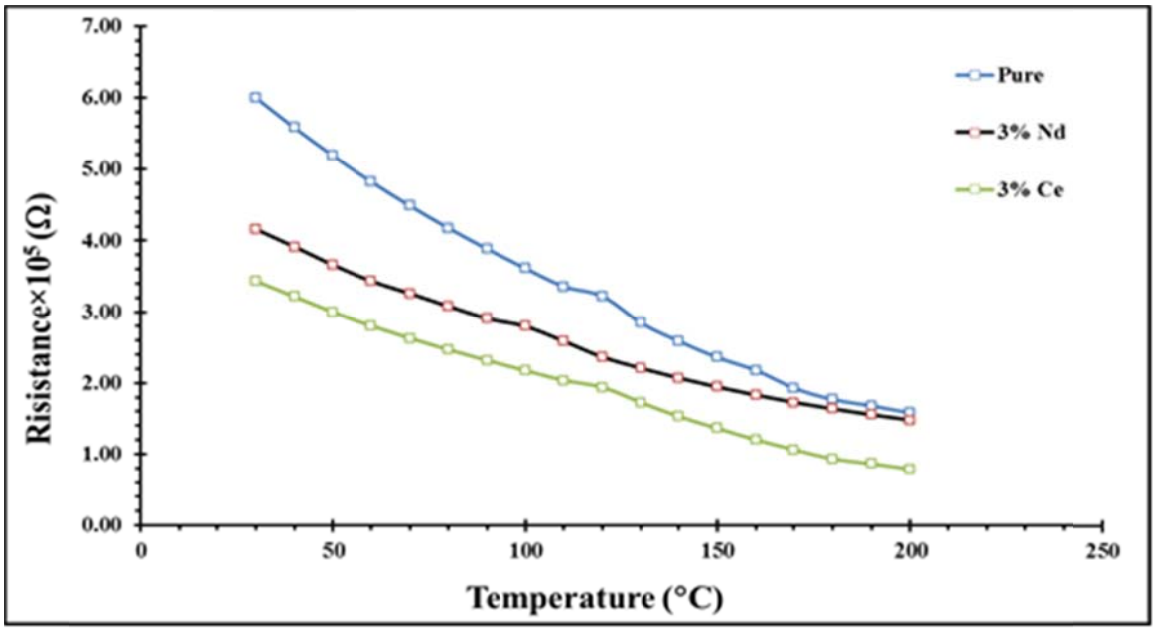

Fig. 4: The variation of resistance as a function to the temperature for un-doped V_2O_5 and doped with different ratio of Nd.

Table 2: D.C activation energies, their ranges and conductivity at room temperature for thin V_2O_5 films at 3% concentration of Nd and Ce.

Sample	E_{a1} (eV)	Temperature Range (K)	E_{a2} (eV)	Temperature Range (K)	σ_{RT} ($\Omega^{-1}.cm^{-1}$)
0%	0.073	303-383	0.186	383-473	0.10417
3% Nd	0.064		0.165		0.16234
3% Ce	0.070		0.182		0.1325

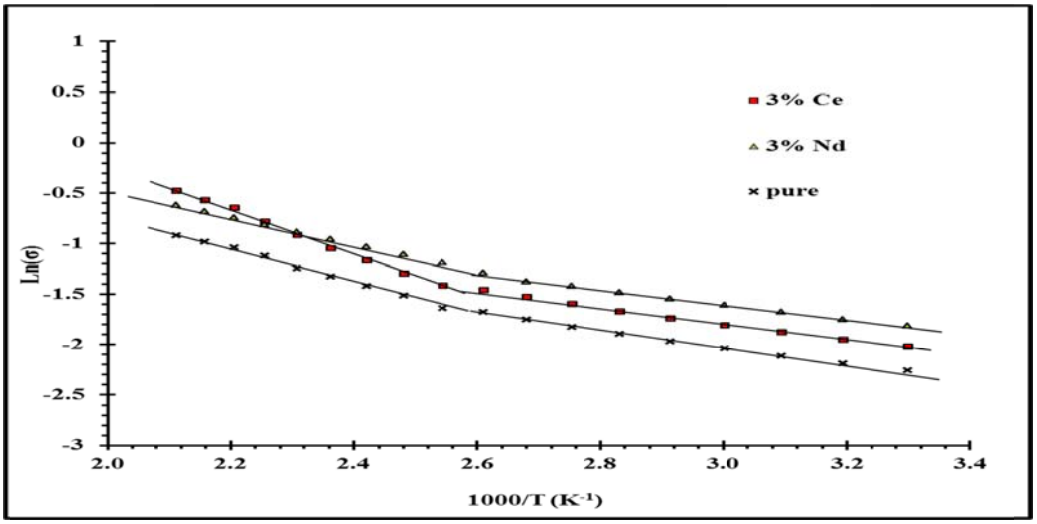

Fig. 5: Plot of ln(σ) vs. 1000/T of un-doped V_2O_5 and doped with 3% ratio of Nd and Ce.

The electrical conductivity (σ) of the films is determined by using the following equation:

$$\sigma = (1/\rho)=L/(R.w.t) \quad (3)$$

where R is the sample resistance, w and t are the width and the thickness of Al electrode of the films and L is the distance between two Al electrodes. The conductivity of un-doped and doped V_2O_5 films are due to the defects such as oxygen vacancies, lattice disorder, etc., which are results

from incomplete oxidation of the films, thus electrical conductivity increases with concentration of oxygen vacancies [27].

The D.C. activation energies calculated from the plot of $\ln(\sigma_{d.c})$ versus 1000/ T, then founded the slope and multiple it by k_β as follow:

$$E_a = k_\beta \cdot \text{slope} \quad (4)$$

Two stages of conductivity throughout the heating temperature range are noted, first activation energy (E_{a1}) occurs at low temperatures near Fermi level within the range (303-383) K, while the second activation energy (E_{a2}) occurs at high temperatures within localized states at the range (383-473) K. This result is in agreement with [28].

Electrical conductivity was increased with Nd and Ce doping concentration which resulting from the increase in the concentration of charge carriers because of the presence of donor levels in the energy gap. While there was decreasing in activation energy with doping concentration at low temperature region. This drop in activation energy may be increased in oxygen vacancies created upon Nd and Ce doping into the V_2O_5 lattice. The low activation energy may be due to the large percentage of highly disordered interfaces. Doping likely increases this disorder, as well as creating more oxygen vacancies for material transport during material synthesis [29]. Higher activation energy at higher temperatures, this is likely due to the segregation of Nd and Ce out of the V_2O_5 lattice structure and into the grain boundaries.

The variation of carriers concentration (n_H) and Hall mobility (μ_H) of un-doped V_2O_5 and doped with Nd and Ce at 3% doping concentration thin films are shown in Table 3.

Hall measurements show that all these films have a negative Hall coefficient (n-type charge carriers), this result was agreement with [5,30]. This is attributed to following two reasons: [31]

i) The number of electrons excited above the conduction band mobility edge is larger than the number of holes excited below the valance band mobility edge.

ii) The life time of free electrons excited from negative defect state is higher than the life time of free holes excited from positive defect state.

It's clear from Table 3 that the carrier concentration increases with dopant ratio of both Nd and Ce while there was decreasing in carrier mobility (μ_H) with Nd and Ce dopant concentration and the doping process did not affect on the type of the charge carriers. The increasing in carrier density with Nd and Ce doping leads to decrease in the resistivity of doped V_2O_5 thin films. It is due to decrease the disorder of the crystal lattice, which causes decreases in phonon scattering and ionized impurity scattering and results in a decrease in mobility [32]. In other words, the reduction in carrier mobility with Nd and Ce doping ratio because of decreasing in crystallite size, as stated in the measurements of X-ray, which in turn leads to an increase in grain boundary and will thus decreasing mobility [33].

Table 3: Hall measurements results of V_2O_5 thin films at 3% dopant ratio of Nd and Ce.

Sample	σ_{RT} ($\Omega^{-1}.cm^{-1}$)	R_H (cm^3/coul)	$n_H \times 10^{15}$ (cm^{-3})	type	μ_H (cm^2/V.sec)
0%	0.1042	-7500	0.833	n	781.25
3% Nd	0.1623	-3750	1.667	n	608.77
3% Ce	0.1325	-3500	1.786	n	463.83

Conclusions

XRD measurement showed that the films to be polycrystalline with orthorhombic phase and with preferred orientation of (010). Analysis of the absorption curves revealed allowed direct transition with optical energy gap 2.34eV. Also, the absorption edge shifts towards higher energies. The absorption edge showed a blue shift, and the optical band gap of the thin films revealed allowed direct transition with optical energy gap 2.2eV. Optical energy gap decreased with doping of both Nd and Ce and with same ratio. The optical transmission of the films increased with doping concentration, which provides a satisfactory optical window for optoelectronic applications. Carrier concentration increases with dopant ratio of both Nd and Ce while there was decreasing in carrier mobility (μ_H) with Nd and Ce dopant concentration and the doping process did not affect on the type of the charge carriers.

References

[1] T. A. A. Hassan, Ph.D Thesis, University of Baghdad, Iraq, 2013.

[2] M. M. Margoni, K. Ramamurthi, S. Mathuri, T. Manimozhi, R. Rameshbabu, K. Sethuraman, Int. J. Chem. Tech Res., 7, 3 (2015) 1072–1078.

[3] M. Benmoussa, A. Outzourhit, A. Bennouna, E. Ameziane, Thin Solid Films, 405, 1–2 (2002) 11–16.

[4] C. W. Zou, W. Gao, Transactions on Electronic Material, 11, 1 (2010) 1–10.

[5] B. M. Mousavi, A. Kompany, Proceedings of the 4th International Conference on Nanostructures (ICNS4), Kish Island, I.R. Iran, 200 (2012) 12–14.

[6] M. E. J. A.Mrigal, M. Addou, S. Khannyra, Int. J. Adv. Res. Phys. Sci., 2, 6 (2015) 24–29.

[7] Y. Vijayakumar, K. N. Reddy, A. V. Moholkar, Mater. Tehnol., 49, 3 (2015) 371–376.

[8]S. Thiagarajan, R. Ganesan, M. Thaiyan, New J. Chem., 39, 12 (2015) 9471–9479.

[9] N. M. Tashtousha, O. Kasasbeh, Jordan J. Pharm. Sci., 6, 1 (2013) 1–8.

[10] S. Beke, L. Korsi, S. Papp, A. Oszk, L. Nnai, Apsusc Appl. Surf. Sci., 255, 24 (2009) 9779–9782.

[11] D. Alamarguy, J. E. Castle, N. Ibris, A. M. Salvi, Surf. Interface Anal., 38, 4 (2006) 801–804.

[12] L. Rivoalen, A. Revcolevschi, J. Livage, R. Collongues, J. Non-Crystalline Solids, 21, 2 (1976) 171–179.

[13] M. A. Kaid, Egypt. J. Solids, 29, 2 (2006) 273–291.

[14] A. Pan, J.-G. Zhang, Z. Nie, G. Cao, B. W. Arey, G. Li, S. Liang, J. Liu, J. Mater. Chem., 20, 41 (2010) 9193.

[15] B. Thangaraju, P. Kaliannan, Crat Cryst. Res. Technol., 35, 1 (2000) 71.

[16] D. Johansson, Ph.D.Thesis, University of Linkopings, Sweden (2011) 67.

[17] A. Chakrabarti, K. Hermann, R. Druzinic, Phys. Rev. B, 59, 16 (1999) 583–590.

[18] V. N. Shevchuk, Y. N. Usatenko, P. Y. Demchenko, O. T. Antonyak, R. Y. Serkiz, Chemistry of Metals and Alloys, 4 (2011) 67–71.

[19] R. L. Josephine, S. Suja, J. Eng. Appl. Sci., 10, 8 (2015) 3713–3716.

[20] K. Hermann, M. Witko, R. Druzinic, A. Chakrabarti, B. Tepper, M. Elsner, A. Gorschlüter, H. Kuhlenbeck, H. J. Freund, J. Electron Spectros. Relat. Phenomena, 98–99 (1999) 245–256.

[21] J. A. Wingrave and C. R. C. Press., "Oxide surfaces." Marcel Dekker, New York, 2001.

[22] M. Benmoussa, A. Outzourhit, R. Jourdani, A. Bennouna, Act. Passiv. Elec. Comp., 26, 4 (2003) 245–256.

[23] Y. Vijayakumar, K. N. Reddy, A.

V. Moholkar, Mater. Technol., 49, 3 (2015) 371–376.
[24] F. Ozutok, K. Erturk, V. Bilgin, Acta Phys. Pol. A, 121, 1 (2012) 221.
[25] N. H. Al-Hardan, M. J. Abdullah, A. A. Aziz, Int. J. Hydrog. Energy, 35, 9 (2010) 4428–4434.
[26] M. Parthibavarman, V. Hariharan; C. Sekar, V.N. Singh, J. Optoelectron. Adv. Mater., 12, 9 (2010) 1894–1898.
[27] S. Chacko, N. Sajeeth Philip, V. K. Vaidyan, Phys. Stat. Solid, 204, 10 (2007) 3305–3315.
[28] C. Londo, V. Hernandez, F. Jurado, Rev. Mex. Phys., 56, 5 (2010) 411–415.
[29] C. Drake, A. Amalu, J. Bernard, S. Seal, J. Appl. Phys., 101, 10 (2007) 104307.
[30] J. Huotari, R. Bjorklund, J. Lappalainen, A. L. Spetz, Pro. Eng., 87 (2014) 1035–1038.
[31] K. S. P. Kumar, Chalcogenide Lett., 4, 5 (2007) 127–132.
[32] H. Kim, C. M. Gilmore, J. Appl. Phys., 86, 11 (1999) 6451– 6461.
[33] I. Akyuz, S. Kose, F. Atay, V. Bilgin, Mat. Sci. Semicond. Process., 13, 2 (2010) 109–114.